12th International Conference on Fracture Mechanics of Concrete and Concrete Structures
FraMCoS-12
B.L.A. Pichler, Ch. Hellmich, P. Preinstorfer (Eds)

https://doi.org/10.21012/FC12.1149
MS09-2:4

ANALYSIS OF DEHYDRATION IN HIGH-PERFORMANCE CONCRETE AT HIGH TEMPERATURE USING NEUTRON RADIOGRAPHY

TAKU KOYAMA[*], MITSO OZAWA[*] AND MANABU KANEMATSU[†]

[*] Gunma University, Program of Civil and Environmental Engineering
1-5-1 Tenjin-cho, Kiryu, Gunma, 376-8515, Japan
e-mail: smallmauntain@gunma-u.ac.jp, ozawa@gunma-u.ac.jp

[†] Tokyo University of Science, Department of Architecture
2641 Yamazaki, Noda, Chiba , 278-8510, Japan
e-mail: manabu@rs.tus.ac.jp

Key words: Spalling, Neutron radiography, High Temperature
Abstract: The aim of this study was to experimentally investigate the dehydration phenomenon of cement-based products in high-performance concrete exposed to high temperatures, using neutron imaging. Graywacke and limestone were employed as coarse aggregates in the high-strength concrete. The results revealed that when one side of a concrete block was heated, dehydration initiated at temperatures exceeding 100°C during the early stages of heating. With prolonged heating, dehydration was observed to begin at temperatures below 100°C. In limestone concrete, the region experiencing dehydration above 100°C extended deeper into the sample compared to that in Graywacke concrete. These findings suggest that the dehydration of cement hydrates under high temperature conditions is influenced by the state of the interface between the coarse aggregate and the cement matrix.

1 INTRODUCTION

Concrete is a fire-resistant material that is widely recognized for fire resistance. However, when concrete is exposed to high temperatures, its chemical and mechanical properties change, leading to damage. Furthermore, high-performance concrete (HPC) exposed to fire often experiences surface explosions [1].

The spalling observed in HPC is believed to result from the combined effects of thermal stress [2] and vapor pressure [3]. Previous studies have investigated the transient thermal strain [4], tensile stress [5], and restraint stress [6] of HPC in high-temperature environments to quantitatively assess thermal stress. To evaluate vapor pressure, sensors have been embedded directly in concrete to measure it, and the hydraulic permeability coefficient [7] as well as pore structure [8] have been analyzed after heating. However, these physical properties were assessed as if the material were homogeneous, without accounting for the heterogeneity of the aggregate and cement matrix.

The deterioration of physical properties and the formation of fine cracks in concrete due to heating result from the contraction of the cement matrix caused by the dehydration of cement hydrate products, as well as the constraint on thermal deformation imposed by the aggregates in the concrete [9–11]. The increase in local water content due to heating contributes to the rise in vapor pressure;

Table 1: Mix proportion.

Weight per unit volume (kg/m3)	
Ordinary Portland Cement	800.0
silica fume	88.9
water	160.0
Sand	425.0
Gravel	1060.2
Superplasticizer	Cx2.7 (%)
antifoam agent	Cx0.7(%)

Table 2: Characteristics of Coarse Aggregate.

	Graywacke	Limestone
Density (g/cm^3)	2.66	2.70
Water absorption rate (%)	0.58	1.32
Thermal expansion coefficient of 20-220°C (μ/°C)	11.8	16.1

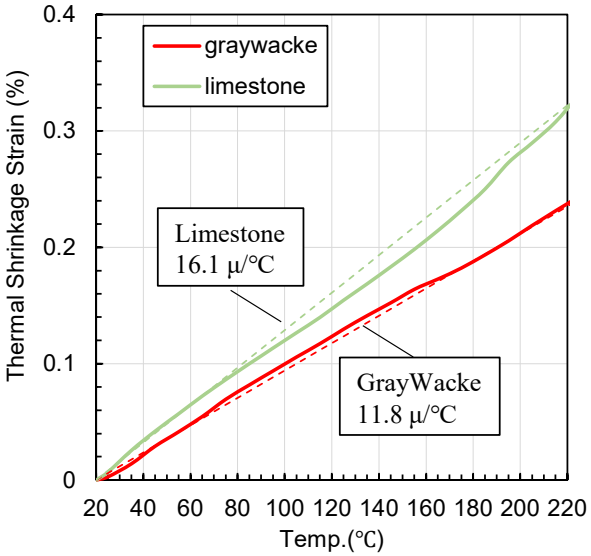

Figure 1: Thermal deformation of coarse aggregate.

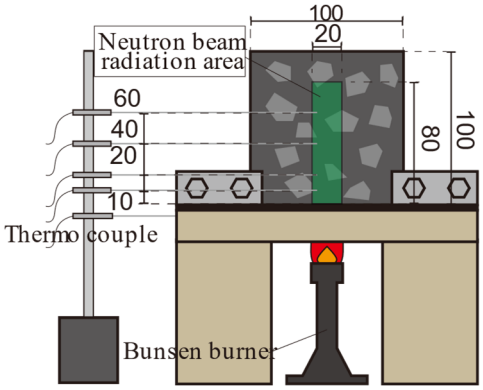

Figure 2: Heating test set up.

however, it is influenced by the water migration from cement hydration to porous media [12].

Therefore, understanding the dehydration profile of concrete due to heating is important for evaluating the thermal stress and vapor pressure.

Neutron imaging has proven effective in evaluating moisture migration in concrete under high-temperature conditions due to its high temporal and spatial resolution [13-14]. Studies have shown that moisture migration progresses from the interface of coarse aggregates [15].

In this study, neutron radiography was used to estimate the dehydration profiles of hydroxides in concrete. The aim was to determine the effect of the type of coarse aggregate on the amount, location, and temperature at which water is removed from the cement hydrates.

2 MATERIALS AND TEST SET-UP

2.1 Specimens and heating set up

Table1 presents the mix proportions of the high-performance concrete, with a water-to-binder (W/B) ratio of 18%. **Table 2** provides the characteristics of the coarse aggregates used. The types of coarse aggregate were hard sandstone and limestone. **Figure 1** illustrates the thermal deformation of the coarse aggregates, as measured by thermomechanical analysis (TMA). The thermal expansion coefficient shown in **Table 2** was calculated based on the thermal expansion observed between 20°C and 220°C.

The high-performance concrete was cast in molds measuring 100 mm × 100 mm × 400 mm. After curing in water for 28 days, the concrete was demolded, and specimens were cut into 20 mm thick sections. These specimens were then stored in a 20°C environment until the start of the experiment. Additionally, they were stored at 20°C for one year. When the specimens were weighed before the experiment, it was same weight as the specimens dried at 105 ℃. It can be

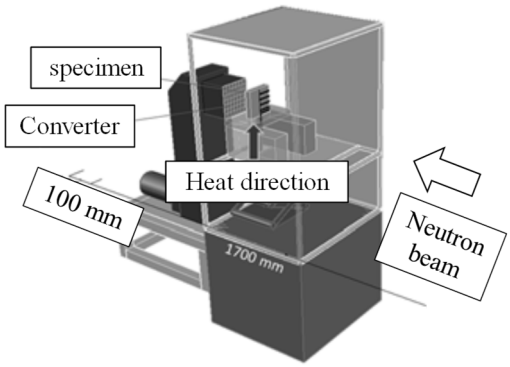

Figure3 : Experimental set up.

inferred that free water in the specimen was less.

Figure 2 illustrates the heating setup. The specimens were heated using a Bunsen gas burner, with the LP gas outflow controlled by a mass flow meter. The internal temperature of the specimens was measured by installing thermocouples in holes positioned at depths of 10, 20, 40, 60, and 80 mm from the heating surface.

The result of heating was constant in seconds from the start of heating then heating surface temperature was about 1000 °C.

2.2 Neutron radiography set up

The experimental setup is shown in **Figure 3**. Neutron radiography (NR) measurements were conducted using the B-4 port of the Kyoto University Research Reactor (KUR) at the Institute for Integrated Radiation and Nuclear Science, Kyoto University.

Neutron beams were utilized during the steady-state operation of the reactor at an output of 1 MW. To account for the influence of scattered neutrons on the specimen, the distance between the specimen and the converter was maintained at 100 mm. The CCD camera's field of view covered an area of 100 × 100 mm, and the spatial resolution of the captured images was approximately 0.1 mm / pixel.

2.3 Imaging analysis

Figure 4 (a) shows a neutron transmission image of the specimen during heating. The transmission image obtained by the NR measurement was 1024×1024 pixel. Moreover, because it was confirmed that neutrons were incident on the position of the image center 20 mm from the incident neutron image (I_0 image), we set the analysis region (ROI), as shown in **Figure.4 (a)**. The white regions displayed in **Figure.4 (a)** indicate areas with a large volume of inclusions relative to the direction of the neutron beam emission, while the black regions represent areas with a higher volume of the matrix. Additionally, dry areas appear whiter in the image.

Figure.4 (b) presents a flow diagram of the image analysis process. The amount of water lost from the concrete during heating can be calculated using **Equation (1)**, which is based on the neutron radiation absorption dose.

$$\Delta - \ln\left(\frac{I}{I_0}\right) = \lambda_w(\rho_w \delta_w) \qquad (1)$$

I is the transmitted neutron beam intensity, I_0 is the incident neutron beam intensity, λ_w is the water mass absorption coefficient, $(\rho_w \delta_w)$ is the amount of dehydration.

Creating the I / I_0 image by dividing the

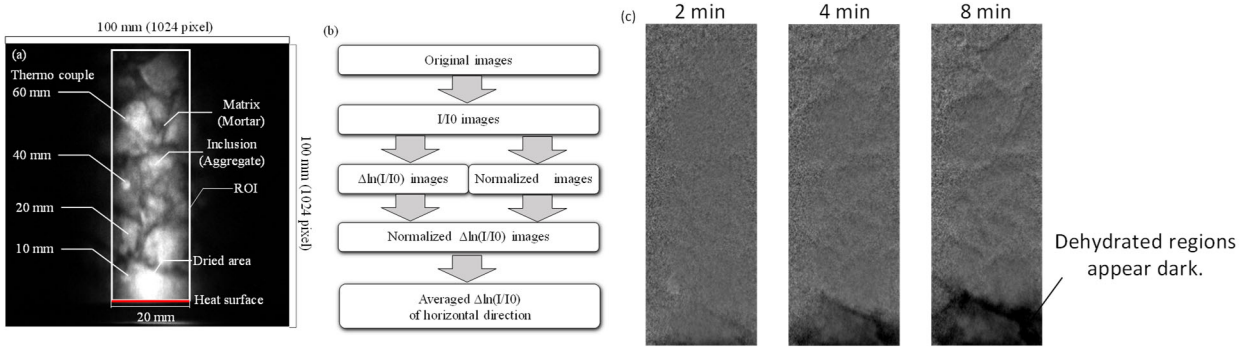

Figure4: (a) Transmission image of specimen (b) and analytical procedure (c) Δln(I/I0) image of HPC dehydrated during heating.

neutron transmission image during heating by an incident neutron image. The I / I_0 image during heating was subtracted from the I / I_0 image of the initial state to create a Δ ln (I / I_0) image, which represents the change in substance quantity. Additionally, a matrix weight distribution image was generated using the initial I / I_0 image. A standardized Δ ln (I / I_0) image was then created by multiplying the Δ ln (I / I_0) image by the matrix weight distribution image [14].

Furthermore, the two-dimensional data were converted into one-dimensional data by averaging along the horizontal direction relative to the heating surface.

Figure 4(c) shows a neutron image of the amount of dehydration at each heating time. From the image, the dehydrated area near the heating surface appears dark, and dehydration progresses deeper into the specimens as the heating time increases.

2.4 Thermogravimetric (TG) analysis

In this study, Thermogravimetric (TG) analysis was conducted using cement paste. The cement pastes, with a water-to-binder (W/B) ratio of 18%, were cast into molds measuring 5 × 5 × 10 mm after mixing. The specimens were removed from the molds after 24 hours, cured in water for 28 days, and then dried for at least 24 hours in a 20°C environment with 0% humidity. A 10 mg powdered sample from the specimens was used for the TG measurement. The TG measurements were performed using a platinum pan, and the analysis was carried out in an open system.

3 RESULTS

3.1 Heat Transfer Analysis

The governing equation for the non-steady-state conduction heat transfer is given by **Equation (2)**.

$$C\dot{T} = \frac{d}{dx}\left(\lambda \frac{dT}{dx}\right) + h\left(T_{sur} - \dot{T}_{bc}\right) \qquad (2)$$

C is the heat capacity, λ is the thermal conductivity, h is the surface heat-transfer coefficient, T_{sur} is the surface temperature of the specimen. A heat transient analysis was performed to clarify the relationship between the loss region of H_2O and the internal temperature of the specimen. The heat capacity and surface heat transfer coefficient in **Equation (2)** were set to approximate the experimental values. Further, the thermal conductivity (λ) was used based on values from a previous study [7], with both heat capacity and thermal conductivity considered as temperature-dependent functions. In this analysis, the surface thermal transfer boundary conditions were applied from the heating surface, and the specimen surface temperature was maintained at a constant 1000°C. The time difference method, combined with the Crank-Nicolson method, was used, with a time width dt = 0.1 ss and an element width dx = 1 mm.

Figure 4 shows the history of the internal temperature of the specimens, while **Figure 5** displays the internal temperature field in the cross-section of the specimen. The circular plots represent the measured values, and the broken lines represent the analytical values. The results showed good agreement between the measured and analytical values up to 260°C, which was measured using a thermocouple installed 10 mm from the heating surface.

Therefore, in this study, the upper limit for the temperature distribution of the test body cross-section shown in Figure 5 is set at 260°C. The relationship between the amount of dehydration and temperature up to 220°C will be discussed.

3.2 Dehydration of concrete measured using neutron imaging

Figure 6 shows the change in the amount of dehydration per unit matrix from the heating surface to a position inside the specimen. Assuming that H_2O is dominant in the amount of mass loss Δln(I/I_0) in the concrete heating experiment up to 260°C, Δln(I/I_0) is the amount of dehydration. From **Figure 6**, it was confirmed that H_2O was dehydrated from the heated surface. As the heating time progressed, dehydration spread to the deeper parts of the

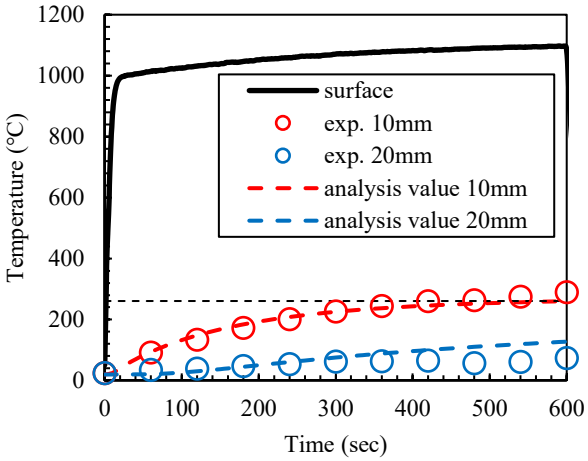

Figure4: History of internal temperature.

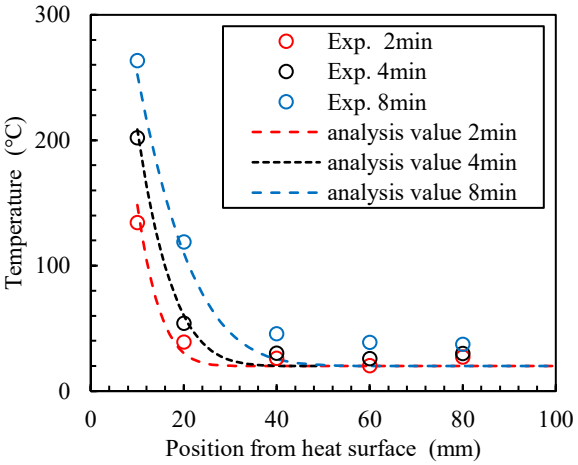

Figure5: Temperature field.

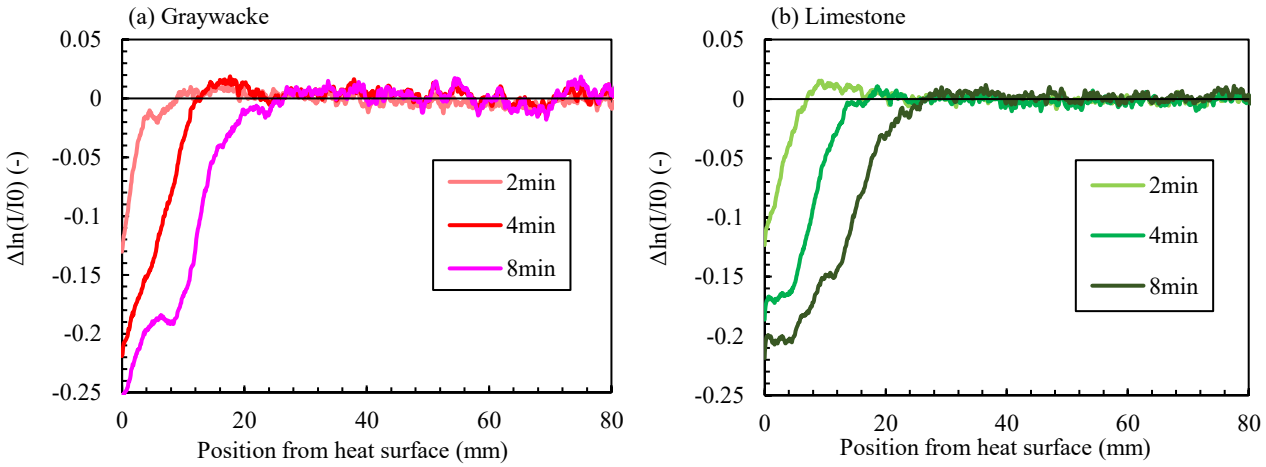

Figure 6: Degrees in the amount of water per unit matrix from the heating surface.

specimen.

To confirm the temperature range in which dehydration occurred, the relationship between the analysis values of the cross-sectional temperature distribution (shown in **Figure 5**) and the amount of dehydration (as shown in **Figure 6**) was plotted. **Figure 7** illustrates the relationship between the amount of dehydration and temperature, as obtained from neutron imaging. The plot shows the measured temperature values from the thermocouples at the 10 mm and 20 mm positions, along with the corresponding amount of dehydration at those positions. It was observed that the temperature range at which dehydration begins is 100°C or higher for both hard Graywacke concrete and limestone concrete, 4 min after heating begins. Furthermore, at 8 min after heating begins, this temperature range shifts to lower temperatures, and dehydration was observed to occur from temperatures below 100°C.

Figure 8 shows the weight loss measured using a powder sample of W/B 18% cement paste obtained from TG measurements. Comparing **Figure 7** and **Figure 8** reveals that the relationship between the dehydration process and temperature differs between the solid and powder samples. Given that no free water exists in any of the samples and that they are in a state of absolute dryness, it is inferred that the observed dehydration is due to the thermal decomposition of the bound water in the C-S-H gel and aluminate phases, such as ettringite. The difference in the temperature at which dehydration begins between the solid and powdered samples is likely attributed to variations in the ease with which water is released, depending on the sample's physical state.

Additionally, the phenomenon that the

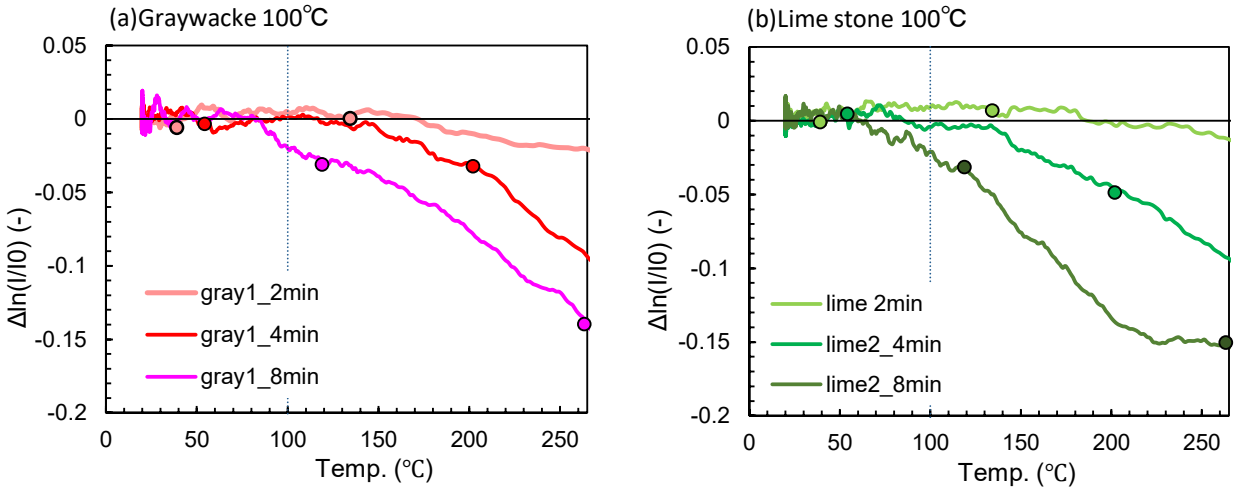

Figure 7: the relationship between the amount of water loss and temperature.

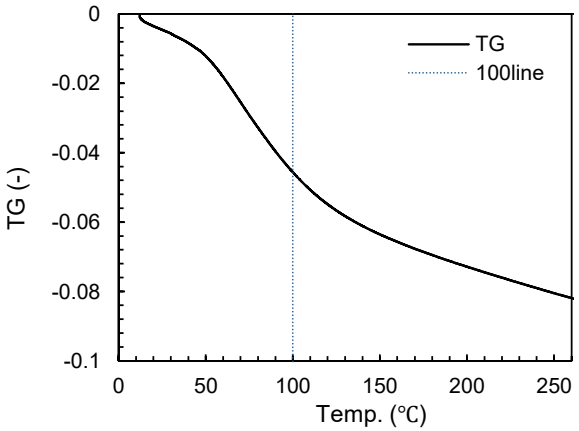

Figure 8 :weight loss measured using a powder sample of W/B 18% cement paste obtained from TG measurement

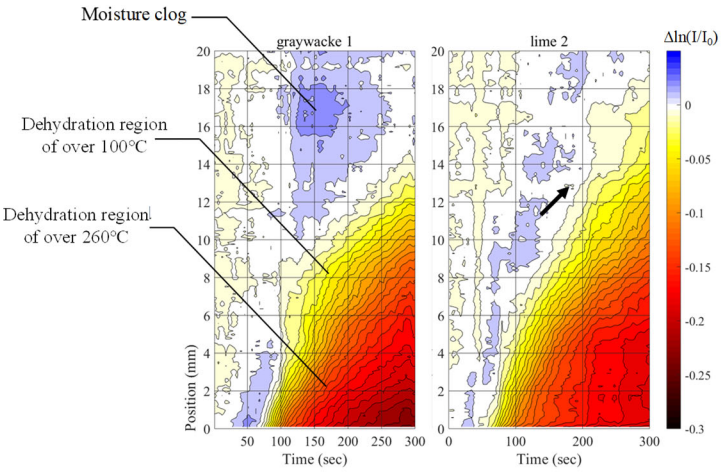

Figure 9: Legend and distribute of amount of substance per matrix unit.

outline of the dehydration process becomes closer to the outline of the TG weight loss rate as the heating time increases suggests that there is water that evaporates at 100℃ or higher, considering the triple point of water.

3.3 Difference of Course aggregate

Figure 9 shows contour plots representing the progression and distribution of the amount of substances per unit matrix. Dewatering is indicated in black, and increasing water content is indicated in blue. **Figure 9** shows that the graywacke concrete has been confirmed to have increased regions of water content (moisture clogs). The moisture clogs with limestone concrete were smaller than those with greywacke concrete. Furthermore, the weight loss of the specimen using limestone was 3.5 g after heating, and the weight loss of the specimen using hard graywacke was 3.0 g. Therefore, it is considered that the specimen that used limestone dissipated moisture more easily than the graywacke specimen.

Using the values derived from the relationship between temperature and the decrease in the amount of substance per unit matrix shown in Figure 7, the color map of the isopleth plot was adjusted. In this adjusted map, the amount of water removed at temperatures of 100°C or higher is indicated in the yellow region, while the amount removed at temperatures of 260°C or higher is shown in the red region. The progression of dehydration in the temperature range of 100°C to 260°C was observed to extend deeper into the specimen over time. Additionally, this area of dehydration

progressed further into the material in concrete using limestone. This behavior is attributed to the fine cracks that develop between the cement matrix and the coarse aggregate layers due to thermal stress, as limestone has a higher thermal expansion coefficient (**Figure 1**). The differences in the thermal expansion coefficients of aggregates can lead to variations in the air permeability of the concrete. This, in turn, affects the dehydration behavior of the cement matrix, creating a gradient in the modulus of elasticity and strength with increasing depth from the heating surface. These gradients may alter the factors contributing to thermal stress, vapor pressure, and other mechanisms responsible for spalling. Therefore, it is suggested that the dehydration of cement hydrates in high-temperature environments is significantly influenced by the state of the interface between the coarse aggregate and the cement matrix.

4 CONCLUSIONS

In this study, neutron imaging was utilized to measure the dehydration profiles of hydrates in high-performance concrete during high-temperature heating. Additionally, a qualitative evaluation was conducted on concrete made from limestone and Graywacke. The findings of this study are summarized as follows:

1. Examination of the relationship between temperatures and the amount of water lost, as measured by neutron imaging, revealed that dehydration begins at temperatures above 100°C in the early stages of heating. As the heating time increases, dehydration shifts to occur at temperatures below 100°C.
2. A comparison between concrete made with limestone and that made with Graywacke indicated that dehydration progressed further into the interior of the concrete made with limestone.

Acknowledgment

This task was carried out by the "Research on unsteady moisture behavior under high-temperature effect of various building materials," at 2018 in Kyoto University of the Institute for Integrated radiation and nuclear science joint-use research issues (30P2-10 representative Dr. M. Kanematsu). We would like to thank Editage (www.editage.jp) for English language editing.

In addition, the authors thank Mr. R. Inose (Flowric Corporation), Ms. M. Sekine (TAIHEIYO Cement Corporation), Mr. K. Ueno (Tokyo University of Science), Dr. T. Noguchi (University of Tokyo), Mr. M. Tamura (University of Tokyo), Mr. Y. Saito (Kyoto University of the Institute for Integrated Radiation and Nuclear Science Joint-Use Research), and Ms. A. Miyabe (Tokyo University of Science).

REFERENCES

[1] Mindeguia J. C. et al, 2010. Temperature, pore pressure and mass variation of concrete subjected to high temperature Experimental and numerical discussion on spalling risk, *Cem Concr Res.*,**40**, **3**, 477-487

[2] Bazant Z.P. 1997. Analysis of Pore Pressure, Thermal Stress and Fracture in Rapidly Heated Concrete, *Proceedings of International Workshop on Fire Performance of High-Strength Concrete, NIST*, Gaithersburg

[3] Ye Li et al, 2021. Pore pressure build-up and explosive spalling in concrete at elevated temperature: A review, *Constr. Build. Mater.* :**284**, 122818

[4] Mindeguia J. C. et al, 2013. Parametrical study of transient thermal strain of ordinary and high-performance concrete, *Cem Concr Res.*, **48**:40-52

[5] Behnood A. et al, 2009. Comparison of compressive and splitting tensile strength of high-strength concrete with and without polypropylene fibers heated to high temperatures, *Fire Saf. J.*, **44**, **8**:1015-1022

[6] Ozawa M. et al, 2018. Behavior of ring-restrained high-performance concrete under extreme heating and development of screening test, *Constr. Build. Mater.* , **162**, **20**: 215-228

[7] Bošnjak J. et al, 2013. Permeability measurement on high strength concrete without and with polypropylene fibers at elevated temperatures using a new test setup, *Cem Concr Res.*, **53**:104-111

[8] Qsymah A. et al, 2017. Micro X-ray computed tomography image-based two-scale homogenization of ultra-high performance fiber reinforced concrete, *Constr. Build. Mater.* , **130**: 230-240

[9] Fu Y. F. et al, 2004. Experimental study of micro/macro crack development and stress–strain relations of cement-based composite materials at elevated temperatures, *Cem Concr Res.*, **34**: 789-797

[10] Fu Y. F. et al, 2004. Thermal induced stress and associated cracking in cement-based composite at elevated temperatures-Part I: Thermal cracking around single inclusion, *Cem. Concr. Compos.* , **26**: 99-111

[11] Fu Y. F. et al, 2007. Numerical tests of thermal cracking induced by temperature gradient in cement-based composites under thermal loads, *Cem. Concr. Compos.*, **29**: 103-116

[12] Zhao J. et al, 2014. A meso-level investigation into the explosive spalling mechanism of high-performance concrete under fire exposure, *Cem Concr Res.*, **65**:64-75

[13] Toropovs N. et al, 2015. Real-time measurements of temperature, pressure and moisture profiles in High-Performance Concrete exposed to high temperatures during neutron radiography imaging, Cem Concr Res., **68**: 166-173

[14] Koyama T. et al, 2016. Effect of The Moisture Movement of The Spalling of HPC under High Temperature, *The 7th International Concrete of Asian Concrete Federation*

[15] Dauti D. et al, 2018. Analysis of moisture migration in concrete at high temperature through in-situ neutron tomography, *Cem Concr Res.*, **111**:41-55